Nano LIFE
Vol. 1, Nos. 3 & 4 (2010) 277–287

DOI: 10.1142/S1793984410000262

World Scientific
www.worldscientific.com

GOLD NANOROD PHOTOTHERMAL THERAPY IN A GENETICALLY ENGINEERED MOUSE MODEL OF SOFT TISSUE SARCOMA

KEVIN Y. LIN[*,¶], ALEXANDER F. BAGLEY[†,¶], ALEXIA Y. ZHANG[‡], DANIEL L. KARL[‡], SAM S. YOON[‡] and SANGEETA N. BHATIA[§,‖]

[*]*Department of Chemical Engineering*
Massachusetts Institute of Technology
77 Massachusetts Avenue, Cambridge, MA 02139, USA

[†]*Division of Health Sciences and Technology*
Massachusetts Institute of Technology
77 Massachusetts Avenue, Cambridge, MA 02139, USA

[‡]*Department of Surgery*
Massachusetts General Hospital and Harvard Medical School
Boston, MA 02114, USA

[§]*David H. Koch Institute for Integrative Cancer Research*
Massachusetts Institute of Technology
77 Massachusetts Avenue, Cambridge, MA 02139, USA
[‖]*sbhatia@mit.edu*

Received 11 March 2011
Accepted 26 June 2011

Plasmonic nanomaterials are poised to impact the clinical management of cancer through their ability to convert externally applied energy into localized heat at sites of diseased tissue. However, characterization of plasmonic nanomaterials as cancer therapeutics has been limited to xenograft models, creating a need to extend these findings to more clinically relevant models of cancer. Here, we evaluate the method of photothermal ablation therapy in a genetically engineered mouse model (GEMM) of sarcoma, which more accurately recapitulates the human disease in terms of structure and biology than subcutaneous xenograft models. Using polyethylene glycol (PEG)-coated gold nanorods (PEG-NRs), we quantitatively evaluate the ability of nanoparticles to penetrate and accumulate in sarcomas through passive targeting mechanisms. We demonstrate that PEG-NR–mediated photothermal heating results in significant delays in tumor growth with no progression in some instances. Lastly, by evaluating our photothermal ablation protocol in a GEMM, we observe off-target heating effects that are not detectable in xenograft models and which may be of future clinical interest.

Keywords: Gold nanorods; photothermal ablation; genetically engineered mouse model.

[¶]These authors contributed equally to this work.
[‖]Corresponding author.

1. Introduction

In the last decade, nanoparticles and nanomaterials have been engineered for a wide array of biomedical applications. The clinical management of cancer stands to benefit greatly from nanoparticles that can more directly and selectively target tumors for diagnosis, imaging, and therapy. Noble metal nanomaterials are especially promising diagnostic, imaging, and therapeutic tools because they exhibit strong optical absorption and scattering properties due to an effect known as surface plasmon resonance. Gold nanoparticles are plasmonic materials which are characterized by facile synthesis and bioconjugation and low cytotoxicity[1–8] and which have demonstrated potential as multimodal diagnostic and therapeutic agents *in vivo*.[7,9,10] As diagnostic agents, gold nanoparticles enable imaging by optical coherence tomography (OCT), photoacoustic tomography, two-photon luminescence, X-ray computed tomography (CT), and surface-enhanced Raman spectroscopy.[4,11–14] Therapeutically, strategies employing gold nanoparticles have harnessed their ability to selectively heat tumor tissue through the localized conversion of light into thermal energy. By varying their geometrical properties, gold nanoparticles, including nanoshells and nanorods, can be tuned to absorb specific near-infrared (NIR) wavelengths, at which biological tissue exhibits relatively low extinction coefficients. Gold nanoparticle–mediated photothermal ablation has shown considerable efficacy in the treatment of cancer, leading to complete resolution of irradiated tumor xenografts in some cases.[6–8] Gold nanoparticle-induced heating has also been combined with other therapeutic modalities to leverage synergies between heat and radiation or chemotherapy, thereby sensitizing tumors to treatment.[15,16] Finally, nanoparticle-induced heating has been used as a photothermal trigger in heat-responsive drug delivery systems.[17,18]

Despite the therapeutic promise of gold nanoparticles, translation to the clinic requires that their effectiveness be validated in physiologically relevant models of human cancer. To date, delivery of gold nanoparticles has been studied in subcutaneous xenograft tumors, and the accumulation of nanoparticles within xenografts has largely relied on passive targeting mechanisms. However, because subcutaneous xenografts fail to recapitulate important structural features of more clinically representative genetically engineered mouse models (GEMMs), the degree to which passive accumulation plays a role in tumor targeting within genetic models remains to be determined.[19–21] In particular, there is increasing evidence that tumor interstitial fluid pressure is model dependent and site specific; therefore, pressure variations between subcutaneous xenografts, orthotopic models, and GEMMs may directly influence the extravasation across the vessel wall, the physical and biological entrapment of nanoparticles in the interstitium, and the intratumoral distribution of gold nanoparticles.[22] Differences in the anatomical location and geometry of the tumor in different mouse models may further affect the ability to focus NIR light, induce specific versus off-target heating, and lethally ablate the tumor. Demonstrating the penetration and accumulation of gold nanoparticles, as well as their ability to induce site-specific photothermal ablation in GEMMs, is therefore an important step as these particles are evaluated for their utility in the clinic.

Here, we sought to directly compare the effectiveness of a polyethylene (PEG)-coated nanorods (PEG-NR) ablative therapeutic protocol in a genetically engineered mouse model to previous results obtained in subcutaneous xenografts.[6–8] To assess the impact of PEG-NR ablative therapy, we selected a model of sarcoma harboring conditional mutations in Kras and Trp53 and resembling human sarcoma both in microscopic structure and by immunohistochemistry.[23] Our lab has previously developed polyethylene glycol (PEG)-coated gold nanorods which exhibit high stability in circulation ($t_{1/2} \sim 17$ h) and a high optical absorption coefficient.[7] Leveraging this technology, we show that intravenously injected PEG-NRs passively accumulate in both subcutaneous xenografts and the sarcoma GEMM. Additionally, NIR laser irradiation results in rapid, sarcoma-specific heating and ablation, leading to significant delays in tumor growth. We further show loss of extremity function due to non-specific heating of the sarcoma, an effect only observed in the GEMM. Collectively, these studies demonstrate that passively targeted PEG-NRs are capable of serving as highly absorbing antennas in a clinically relevant model of cancer, and suggest that an optimal combination of PEG-NR delivery and appropriate ablation protocol could be translated to clinical utility.

2. Materials and Methods

2.1. *Preparation of PEG-coated gold NRs*

Gold nanorods were prepared as described previously.[7] Briefly, $\sim 10 \times 40$ nm cetyltrimethylammonium bromide (CTAB)-coated gold NRs with longitudinal plasmon resonance at 810 (Nanopartz Inc.) were centrifuged at 16,000 rcf to concentrate and resuspended in 100 μM of 5-kDa methyl-PEG-thiol (Layson Bio, Inc.). The solution of 5-kDa methyl-PEG-thiol and CTAB-coated gold NRs was mixed and dialyzed overnight against ultrapure water (18 MΩ cm^{-1}) using cellulose ester membrane dialysis (Spectrapor). Dialyzed samples were washed and filtered through 100-kDa filters (Millipore) to remove excess polymer, resuspended in PBS, and stored at 4°C.

2.2. *Generation of soft tissue sarcomas*

The mouse model of sarcoma was described previously by Kirsch *et al.*[23] The 129 S_4/SvJae mouse strain was bred and used for the generation of transgenic sarcoma mice. These mice harbor the following conditional mutations: LSL-Kras$^{G12D/+}$ and p53$^{Fl/Fl}$. Soft tissue sarcomas were generated by intramuscular injection of 2.4×10^7 pfu of adenovirus (Ad-Cre) expressing Cre-recombinase (Gene Vector Transfer Core, University of Iowa) in the lower extremity. All animal studies and procedures were approved by the MIT and MGH Institutional Animal Care and Use Committees.

2.3. *Generation of HT-1080 xenografts*

To generate subcutaneous xenograft models, nude mice (Jackson Labs) were injected bilaterally in the hind flanks with $\sim 5 \times 10^6$ HT-1080 cells suspended in 200 μL DMEM.

2.4. *Silver enhancement staining*

Paraffin-embedded tissue sections were dewaxed and rinsed with double-distilled water for up to 30 sec. Silver enhancement was performed using the Silver Enhancer Kit for Membranes (Cytodiagnostics). Equal volumes of Silver Enhancer Solution A and Silver Enhancer Solution B were mixed, and 50−100 μL was added to tissue sections, ensuring that the entire tissue was covered. Several dilutions of Solution A/Solution B mixtures in double-distilled water were tested. To determine the optimal enhancement time, representative 20X fields were imaged every 10 min for up to 80 min (Nikon ECLIPSE Ti). After incubation in silver enhancement solution, tissues were rinsed well with double-distilled water for up to 60 sec. Samples were counterstained with hematoxylin, dehydrated, and mounted using standard protocols.

Quantification of silver deposits was performed using ImageJ software. To generate particle counts, the Analyze Particles command was applied to each contrast-enhanced, 8-bit, thresholded image. The same thresholding values were applied to all images included in the analysis.

2.5. *ICP-MS*

Samples for inductively coupled plasma mass spectrometry, or ICP-MS analysis, were frozen, lyophilized, and dissolved in aqua regia, prepared by adding 100 μL of HNO_3 to 300 μL of 37% HCl for 72 h to dissolve gold particles. Then, samples were diluted to 10 mL with 9.6 mL of 2% HNO_3 and analyzed via ICP-MS against standards (ThermoScientific Finnigan ELEMENT2). Control saline and organ samples with exogenously added GNRs were used for calibration.

2.6. *In vivo photothermal therapy*

Approximately 90 days after injection of Ad-Cre, mice bearing sarcomas between 150−200 mm^3 were randomized into one of three groups: PEG-NR + NIR, PEG-NR only, and NIR only ($n = 4$−5 mice per group). Mice were then injected through the tail vein with PEG-NRs in PBS (40 mg Au/kg). After allowing 72 h for vascular clearance of PEG-NRs, the mice were anaesthetized with ketamine/xylazine and sarcomas were irradiated with a NIR laser ($\sim$0.5 W/cm^2, 810 nm, $\sim$1-cm beam diameter). Prior to irradiation, the area around the tumor was shaved to remove excess hair. To monitor surface temperature during irradiation, an infrared thermographic camera (FLIR, Thermacam S60) was used. To assess tumor growth following treatment, tumors were measured every two to three days using digital calipers. Mice were euthanized when tumors exceeded 15 mm in any single dimension.

2.7. *Immunohistochemistry*

Immunohistochemistry was performed as described previously.[24] Briefly, immunostaining was performed on formalin-fixed paraffin embedded sections following antigen retrieval (10 mM citrate buffer (pH ~ 6.0) at 95°C for 20 min; 22°C for 20 min). Primary antibodies rat anti-mouse CD31 (1:100, Pharmingen, San Jose, CA, USA) and mouse anti-PCNA (1:500, PC-10; Santa Cruz Biotechnology, Santa Cruz, CA, USA) were applied to tissue sections for 1 h at room temperature. Secondary antibodies were applied for 30 min at room temperature: biotinylated rabbit anti-rat IgG (1:1000, Vector Laboratories, Burlingame, CA, USA) or biotinylated horse anti-mouse IgG (1:1000, Vector Laboratories, Burlingame, CA, USA). Sections were then incubated for 30 min with ABC reagent (Vector Laboratories, Burlingame, CA, USA), rinsed with PBS-T, and incubated in DAB chromagen reagent (Vector Laboratories, Burlingame, CA, USA). The sections were rinsed under running tap water for 5 min and counterstained in Mayer's Hematoxylin (Sigma, St. Louis, MO USA), dehydrated, and mounted using Permount (Fisher Scientific, Pittsburgh, PA, USA). Standard hematoxylin and eosin (H&E) staining was performed on tissue sections.

3. Results

3.1. *Sarcoma treatment and experimental schedule*

Sarcoma-bearing mice were injected with either PEG-NRs or PBS control and subjected to the photothermal ablation protocol [Fig. 1(a)]. Following irradiation, mice in the treatment trial were regularly monitored for tumor burden. A second group of mice was sacrificed either 24 or 72 h after ablation to assess the short-term histopathological effects of ablation. We verified the uniform structure of PEG-NRs by transmission electron microscopy [Fig. 1(b)] and demonstrated the capacity of PEG-NRs to specifically and significantly heat sarcomas exposed to NIR irradiation [Figs. 1(c) and 1(d)]. A representative photograph of the sarcoma [Fig. 1(e)] provides perspective on the challenges of locally specific ablation and the potential source for non-specific heating effects [Figs. 1(d) and 1(e), Supp. Fig. 1].

3.2. *Comparison of PEG-NR accumulation in GEMM and xenograft models of sarcoma*

To confirm the presence of PEG-NR accumulation in the tumor interstitium of both the GEMM and

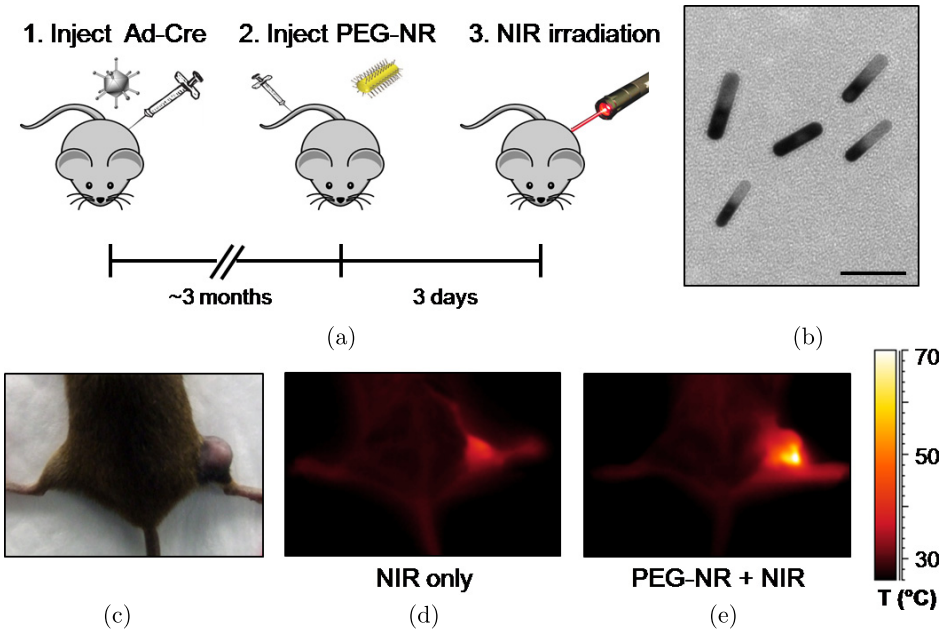

Fig. 1. Schematic of GNR heating with NIR laser irradiation in a GEMM of sarcoma. (a) Timeline of sarcoma generation and photothermal ablation procedure. (b) TEM image of PEG-NRs. Scale bar represents 50 nm. ((c), (d), (e)) Bright field (c) and IR thermographic images of mice with NIR irradiation only (d) and PEG-NR + NIR irradiation (e).

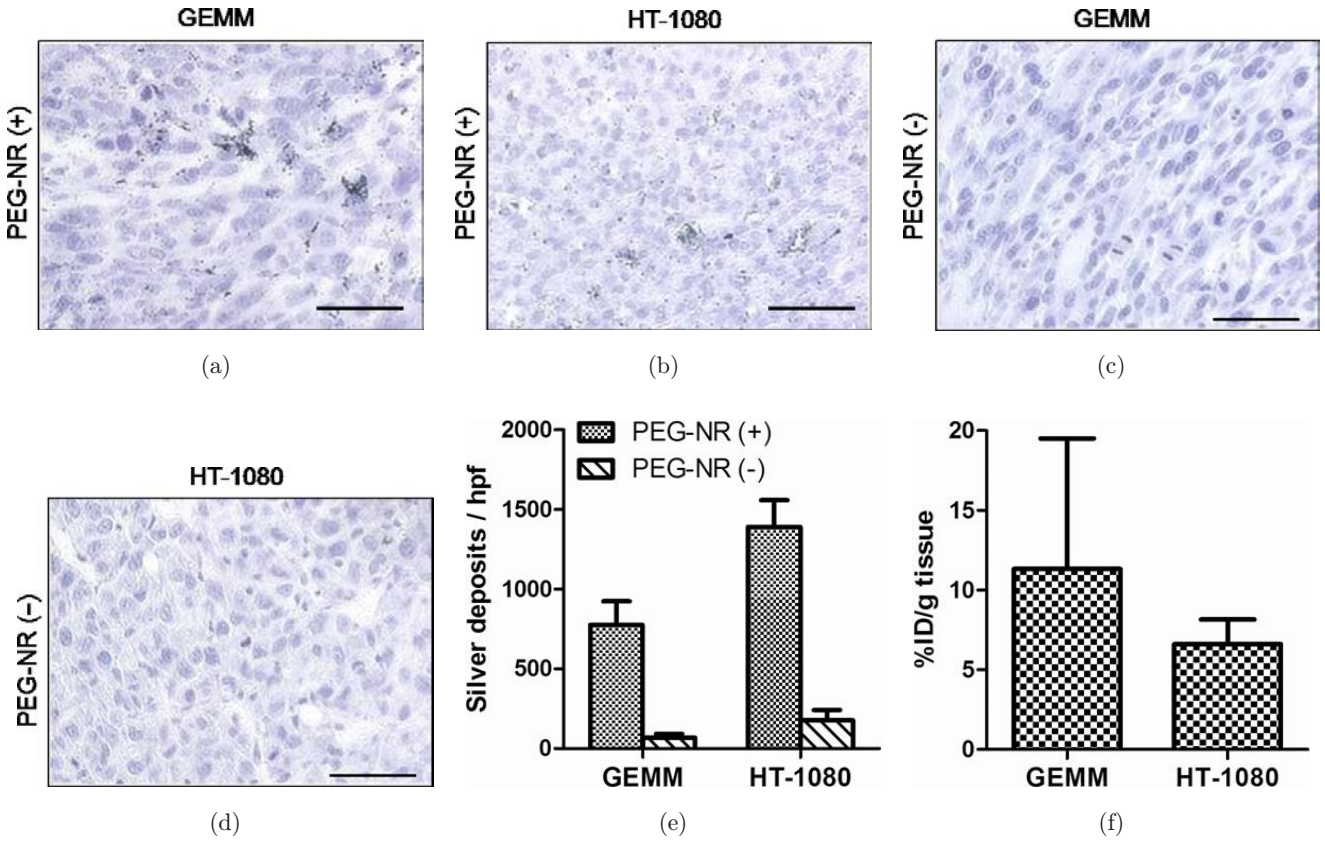

Fig. 2. Accumulation of PEG-NRs in GEMM and subcutaneous xenograft. Representative silver enhancement staining of PEG-NRs in a GEMM of sarcoma (a) and HT-1080 xenograft (b). Representative silver enhancement staining in an uninjected GEMM of sarcoma (c) and HT-1080 xenograft (d). Scale bar represents 50 μm. (e) Quantification of silver enhanced spots. Contrast-enhanced images captured at 20× magnification were analyzed on ImageJ software ($n = 9$ per group). (f) ICP-MS quantification of PEG-NR deposition in GEMM of sarcoma and HT-1080 xenografts 72 h after intravenous administration.

xenograft, we performed silver enhancement staining on tumor sections to visualize PEG-NR microdistribution within the tumors. Both the GEMMs and HT-1080 xenografts displayed comparable PEG-NR microdistributions, with PEG-NRs appearing throughout the tumor tissue [Figs. 2(a) and 2(b)], while control samples displayed little to no detectable background staining [Figs. 2(c) and 2(d)]. Quantification of silver-enhanced PEG-NRs in histological sections revealed a greater number of particles accumulating in the HT-1080 xenografts compared to the GEMM; further, both the HT-1080 xenografts and GEMMs exhibited significant accumulation of particles relative to uninjected tumor controls [Fig. 2(e)]. Additionally, we did not detect significant silver deposits in surrounding tissues, including skeletal muscle, indicating that PEG-NRs accumulated preferentially in sarcomas (Supp. Fig. 2). ICP-MS confirmed the presence of gold in the GEMMs (6.60 %ID/g) in amounts comparable to those seen in the HT-1080 xenografts (11.32 %ID/g) [Fig. 2(f)]. These results directly confirm that PEG-NRs are able to penetrate and accumulate in sarcoma GEMMs in amounts sufficient for photothermal ablation protocols.

3.3. *Immunohistochemistry of tumors following photothermal ablation*

Examination of H&E-stained paraffin sections revealed regions of gross necrosis at 24 and 72 h post-irradiation. These sections were characterized by loss of tumor architecture, cellularly hypodense regions, lymphocytic infiltrates, and irregular nuclear staining patterns (Fig. 3 and Supp. Fig. 3). These regions likely correspond to the portions of the tumor receiving the majority of photothermal energy during the ablation procedure.

To assess cellular proliferation, we immunohistochemically stained the sarcoma sections for

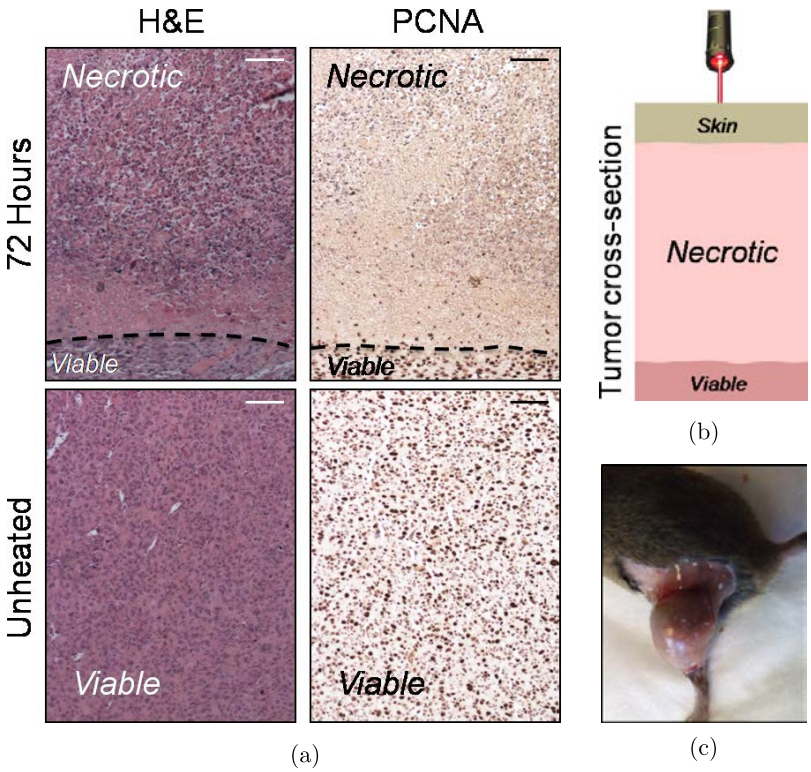

Fig. 3. Immunohistochemical analysis of short-term heating effects on GEMM of sarcoma. (a) H&E and PCNA staining of sarcoma 72 h after heating versus an unheated control. Scale bar represents 100 μm. Contrast-enhanced images captured at 10× magnification. (b) Schematic of sarcoma cross-section following heating. (c) Photograph of PEG-NR + NIR treated sarcoma prior to excision, 72 h post-heating.

proliferating cell nuclear antigen (PCNA). Consistent with the H&E results, we observed wide regions of absent PCNA staining throughout the tumors at 24 and 72 h following ablation (Fig. 3). Interestingly, we identified isolated regions located exclusively at sites of the tumor most distal from the skin surface that stained positively for PCNA. These areas of viable tissue account for anywhere between 0% to approximately 20% of the area of some tissue sections (Supp. Fig. 3), suggesting that some portions of the tumor did not receive sufficient photothermal energy during the ablation procedure.

Finally, to understand how photothermal ablation influences the distribution of blood vessels in the sarcoma, we measured expression of CD31, an endothelial cell marker commonly used to identify blood vessels. Necrotic regions exhibited diffuse, non-specific staining patterns bearing no resemblance to the blood vessels observed in untreated control tissue (Supp. Fig. 4). Thus, in regions of tumor receiving sufficient irradiative heat to induce necrosis, the tumor-associated vasculature is also ablated.

3.4. *Therapeutic assessment of photothermal ablation in a transgenic sarcoma model*

To test the ability of a single dose of PEG-NRs to significantly delay tumor growth following one session of near-IR irradiation, genetically modified 129 S_4/SvJae mice-bearing-induced soft tissue sarcomas were injected with PEG-NRs. Mice were randomized to one of three cohorts (PEG-NRs + NIR, PEG-NRs only, NIR only). After plasma clearance of PEG-NRs, tumors in the PEG-NRs + NIR and NIR only groups were irradiated for 5 min (~0.5 W/cm^2, 810 nm) and tumor volume was measured over time [Fig. 4(a)]. Mice receiving the PEG-NRs + NIR treatment experienced significant tumor growth delay and extended lifespan compared to control treatment groups. During the post-ablation observation period, all mice in the PEG-NR−only and NIR only groups developed substantial tumor burdens requiring euthanization by day 16, whereas mice receiving PEG-NRs + NIR survived until day 30 or longer [Fig. 4(b)]. At the end of the study period, the

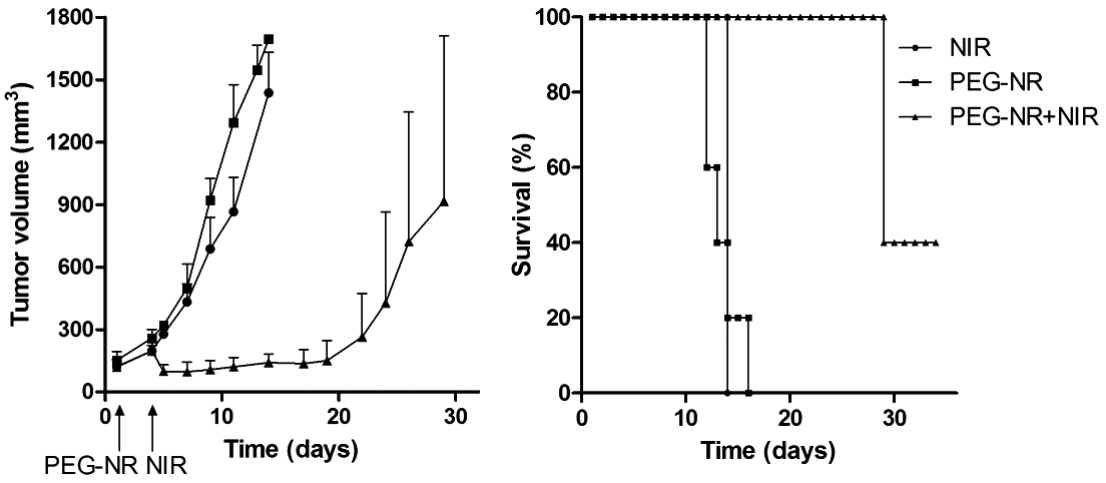

Fig. 4. Photothermal ablation of GEMM of sarcoma using PEG-NRs. (a) Volumetric changes in tumor volume are plotted over time ($n = 4–5$). Error bars represent standard deviations. PEG-NR is statistically different from NIR and PEG-NR from day 7 onwards with $p < 0.0001$ based on analysis of variance. (b) Survival of mice over time ($n = 4–5$).

two remaining mice had tumor volumes $< 150\,\text{mm}^3$ (Supp. Fig. 5). Notably, four of the five mice receiving PEG-NR + NIR lost lower extremity function after the ablation procedure. Additionally, in a repeat therapeutic trial, we observed delayed progression of sarcoma consistent with our initial results.

4. Discussion

Surgery, chemotherapy, and radiation have remained the standard of care in cancer therapy for decades. Novel approaches harnessing the unique properties of nanomaterials have been proposed to improve cancer therapy in the future. To date, numerous therapeutic protocols, involving a variety of nanomaterials, have been described in xenograft mouse models. While xenograft models offer a straightforward and reliable method for quantitatively assessing tumor burden, studies in more physiologic tumor microenvironments, such as those that occur in GEMMs, may be more accurate predictors of therapeutic efficacy.[25] For these reasons, GEMMs are gaining favor in the pharmaceutical industry and will almost certainly find utility in assessing the clinical validity of nanomaterial-based therapeutic protocols as well.

This study represents the first demonstration of a therapeutic, nanoparticle-mediated thermal ablation protocol in a GEMM. We have demonstrated that PEG-NRs accumulate in the sarcomas at levels comparable to those in subcutaneous HT-1080 xenografts. Deposition of PEG-NRs is sufficient to facilitate photothermal ablation of the sarcomas upon localized administration of near-infrared irradiation.

Although numerous lines of evidence support the notion that passively targeted nanotherapeutics can penetrate and accumulate in human tumors, this phenomenon has not been well characterized in a clinical setting.[26,27] Routinely used xenograft models fail to capture important characteristics of human disease that may impact the effectiveness of passive targeting mechanisms.[19] This uncertainty is significant as many nanotherapeutic approaches rely on passive targeting to varying degrees in order for the therapeutic payload to accumulate at the site of disease. Our demonstration of untargeted PEG-NR accumulation in a GEMM of sarcoma provides evidence that passive targeting is indeed sufficient for PEG-NRs to accumulate in a physiologic tumor microenvironment.

The considerable heterogeneity of human cancers is an important factor for PEG-NR-based therapies. It is not anticipated that a "one-size-fits-all" therapy will be identified, but rather that therapeutic protocols must be tailored to each type of cancer. Features including grade, stage, tissue of origin, anatomical location, and metastatic progression will influence if, and to what extent, PEG-NR-based therapies will have a place in the clinic.[23,28,29] For example, because of constraints related to depth of NIR irradiation into tissues,

tumors that develop close to the skin surface, such as some soft tissue sarcomas, would be better candidates for PEG-NR-based therapies than tumors that develop at sites more distant from the skin surface. Interestingly, in our GEMM, a portion of the sarcoma developed closer to the surface while the remainder developed deeper within surrounding skeletal muscle. In contrast to HT-1080 xenograft models which replicate superficial truncal tumors, our GEMM replicates a deep extremity sarcoma, which represents the majority of human sarcomas. We propose that this spatial heterogeneity contributed to the differential success in ablative therapy that we observed. Additionally, tumors that are identified at earlier stages may be better candidates for PEG-NR therapies than tumors identified at late stages, such as pancreatic adenocarcinoma,[30] because of the increased challenge of optimally irradiating multiple metastatic lesions.

Notably, a significant proportion of mice to undergo photothermal ablation lost function in the irradiated limb following treatment. Because the sarcomas invade surrounding skeletal muscle, the thermal energy generated within the sarcoma damaged the skeletal muscle as well as the sciatic and femoral nerves in the leg. We believe this observation is important in two respects. First, it suggests that improvements are required in the irradiation protocol to provide more precise thermal ablation at cellular resolution. Pulsed laser sources represent one possibility for improving the localization of photothermal ablation. Second, this unwanted side effect of the therapy could only be detected and fully appreciated in a GEMM, in which the sarcoma's anatomical location closely mimics that of human extremity soft tissue sarcomas. While a subcutaneous xenograft model can provide important information such as tumor burden in response to treatment, only in a GEMM can these realistic clinical consequences be detected and assessed.

5. Conclusion

The ability of mouse models to accurately recapitulate human cancers and yield clinically insightful results is critical to the continuing development of nanotechnology for therapy and diagnostics. Our work highlights the therapeutic efficacy and potential challenges of PEG-NR–mediated photothermal ablation therapy in a GEMM of sarcoma. We anticipate that our findings will enable the development of improved therapeutic protocols as PEG-NRs and other nanotherapeutics advance closer to clinical use.

Acknowledgments

This project was supported by the MIT-MGH Collaborative Initiative in Translational Cancer Research and the NIH (R01 CA124427). S. B. is an HHMI investigator. A.F.B. acknowledges support from the NIH/Medical Scientist Training Program. The authors would like to acknowledge Dr. Alice Chen for her helpful suggestions on the manuscript. The authors also thank Matt Kinsella for assistance with ICP-MS, Prof. Warren Chan for assistance with silver enhancement staining, Prof. Yoel Fink for use of the IR camera, and Nicki Watson for TEM images. Histology support from the Koch Institute Histology Core Facility was provided by Michael Brown.

References

1. R. Elghanian, J. J. Storhoff, R. C. Mucic, R. L. Letsinger and C. A. Mirkin, *Science* **277**, 1078 (1997).
2. D. S. Grubisha, R. J. Lipert, H.-Y. Park, J. Driskell and M. D. Porter, *Anal. Chem.* **75**, 5936 (2003).
3. J. B. Jackson, S. L. Westcott, L. R. Hirsch, J. L. West and N. J. Halas, *Appl. Phys. Lett.* **82**, 257 (2003).
4. X. Qian *et al.*, *Nat. Biotech.* **26**, 83 (2008).
5. L. R. Hirsch *et al.*, *Proc. Nat. Acad. Sci. USA* **100**, 13549 (2003).
6. D. P. O'Neal, R. H. Leon, J. H. Naomi, J. D. Payne and L. W. Jennifer, *Cancer Lett.* **209**, 171 (2004).
7. G. von Maltzahn *et al.*, *Cancer Res.* **69**, 3892 (2009).
8. B. E. Dickerson *et al.*, *Cancer Lett.* **269**, 57 (2008).
9. A. M. Gobin *et al.*, *Nano Lett.* **7**, 1929 (2007).
10. G. von Maltzahn *et al.*, *Adv. Mater.* **21**, 3175 (2009).
11. J. Chen *et al.*, *Nano Lett.* **5**, 473 (2005).
12. Y. Wang *et al.*, *Nano Lett.* **4**, 1689 (2004).
13. H. Wang *et al.*, *Proc. Natl. Acad. Sci. USA* **102**, 15752 (2005).
14. D. Kim, S. Park, J. H. Lee, Y. Y. Jeong and S. Jon, *J. Am. Chem. Soc.* **129**, 7661 (2007).
15. J.-H. Park *et al.*, *Proc. Natl. Acad. Sci.* **107**, 981 (2010).
16. R. L. Atkinson *et al.*, *Sci. Transl. Med.* **2**, 55ra79 (2010).
17. J.-H. Park *et al.*, *Adv. Mater.* **22**, 880 (2010).
18. M. S. Yavuz *et al.*, *Nat. Mater.* **8**, 935 (2009).
19. O. J. Becher, E. C. Holland, E. A. Sausville and A. M. Burger, *Cancer Res.* **66**, 3355 (2006).

20. E. A. Sausville, A. M. Burger, O. J. Becher and E. C. Holland, *Cancer Res.* **66**, 3351 (2006).
21. K. K. Frese and D. A. Tuveson, *Nat. Rev. Cancer* **7**, 654 (2007).
22. C. Brekken, O. Bruland and C. de Lange Davies, *Anticancer Res.* **20**, 3503 (2000).
23. D. G. Kirsch *et al.*, *Nat. Med.* **13**, 992 (2007).
24. S. S. Yoon *et al.*, *Int. J. Radiation Oncol. Biol. Phys.* **74**, 1207 (2009).
25. M. Singh *et al.*, *Nat. Biotech.* **28**, 585 (2010).
26. J. Fang, H. Nakamura and H. Maeda, *Adv. Drug Deliv. Rev.* **63**, 136 (2011).
27. M. E. Davis, Z. Chen and D. M. Shin, *Nat. Rev. Drug Discov.* **7**, 771 (2008).
28. M. Nogawa *et al.*, *Cancer Lett.* **217**, 243 (2005).
29. J. K. Mito *et al.*, *PLoS One* **4**, e8075 (2009).
30. M. Hidalgo, *New Eng. J. Med.* **362**, 1605 (2010).

Supplementary Information

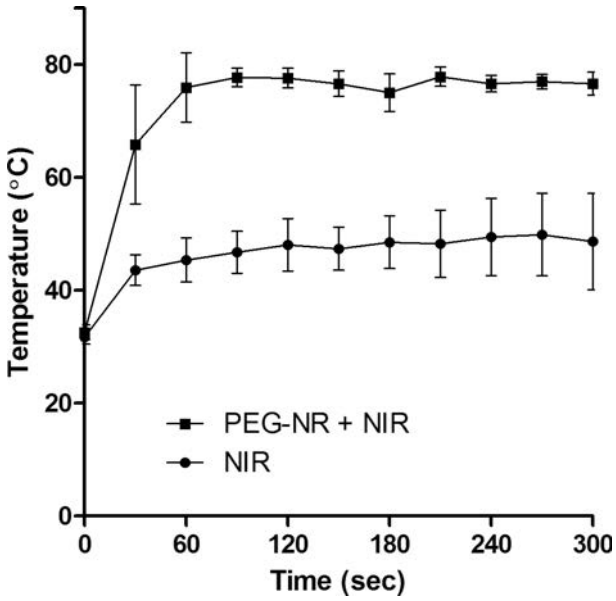

Fig. 1. Temperature profile of GEMM of sarcoma heating with and without PEG-NR ($n = 4$ or 5). Error bars represent standard deviations. Temperatures are statistically different at each time point from 30−300 s with $p < 0.005$ based on Student's t-test.

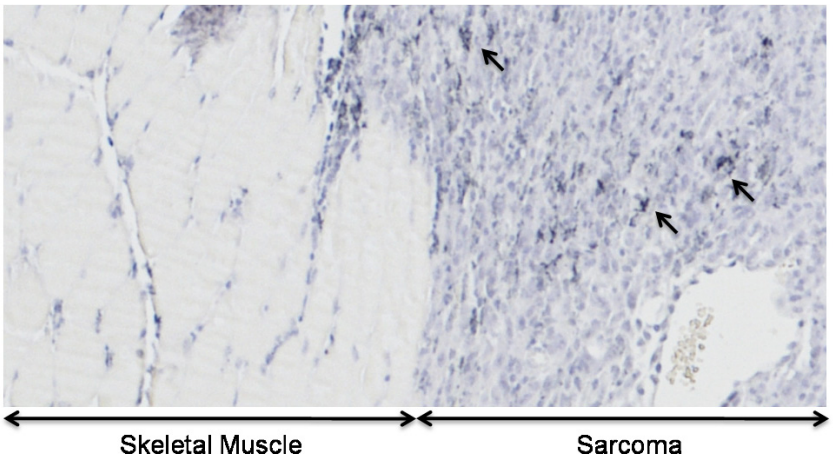

Fig. 2. Silver enhancement staining with H&E counterstaining in a sarcoma tissue section from a mouse injected with PEG-NR reveals silver deposits present in the sarcoma but absent in adjacent skeletal muscle. Silver deposits are indicated by arrowheads. Images were acquired at 4× magnification.

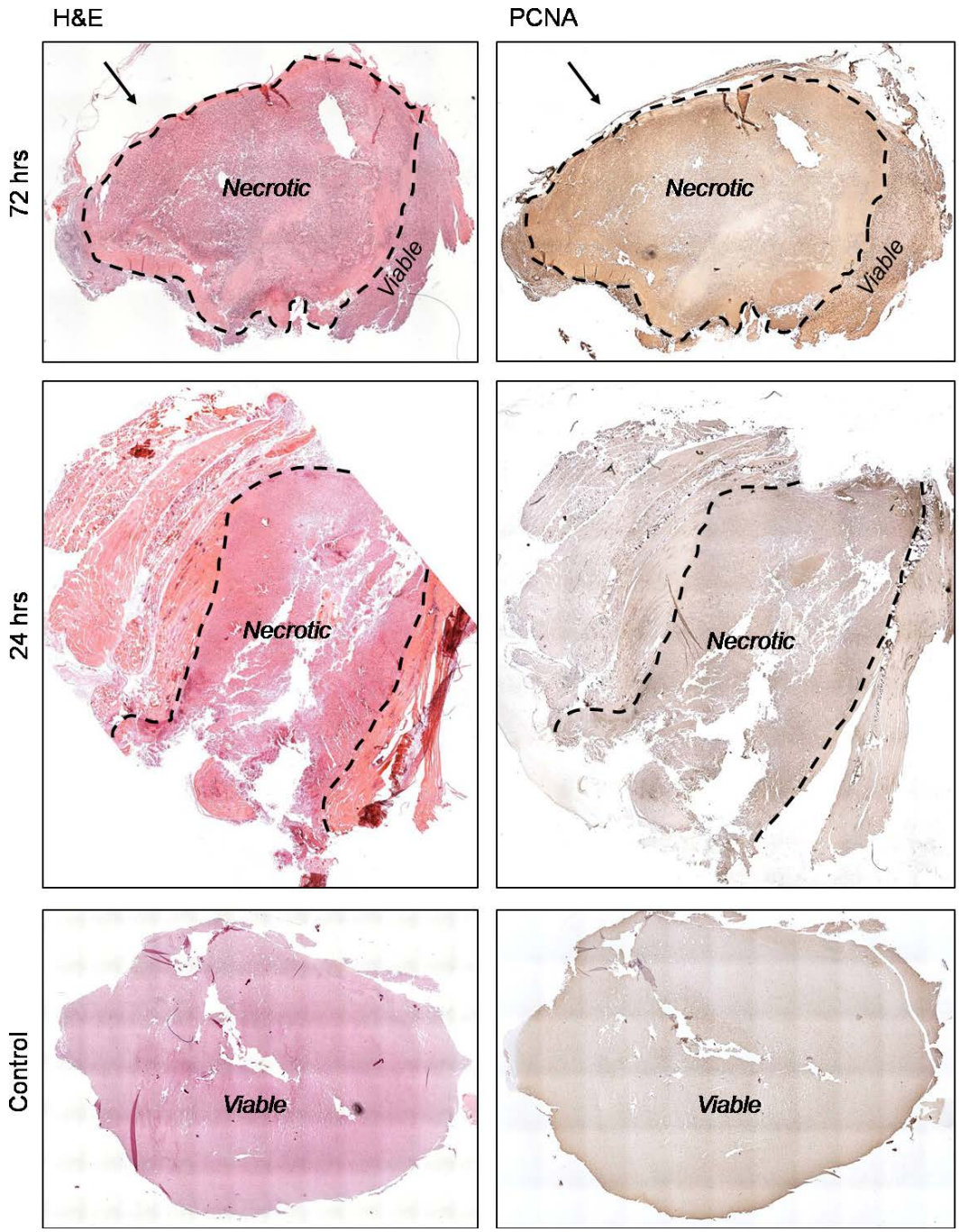

Fig. 3. Immunohistochemical analysis of short-term heating effects on GEMM of sarcoma. Scale bar represents 50 μm. Contrast-enhanced images captured at 20× magnification. Arrow indicates the direction of NIR irradiation.

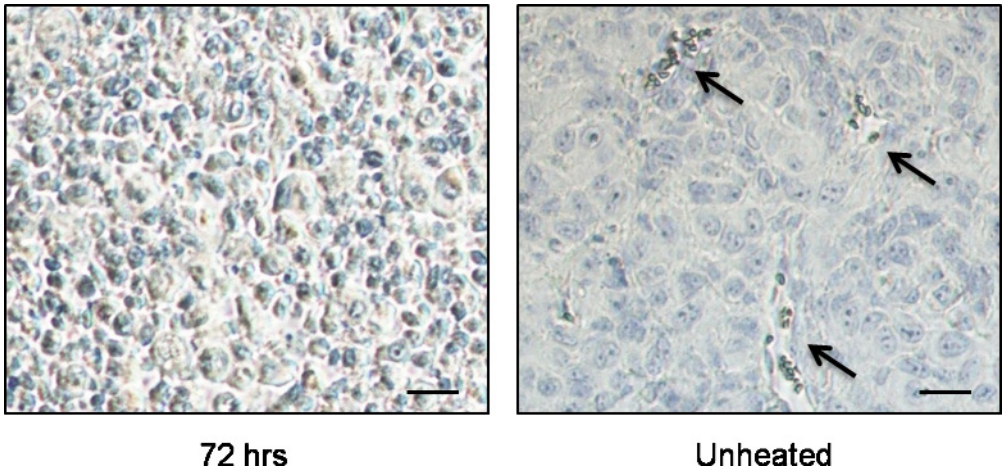

Fig. 4. Immunohistochemical analysis of short-term heating effects on GEMM of sarcoma. CD31 staining of tumor vessels at 72 h after heating and in an unheated control. Scale bar represents 50 μm. Contrast-enhanced images captured at 20× magnification.

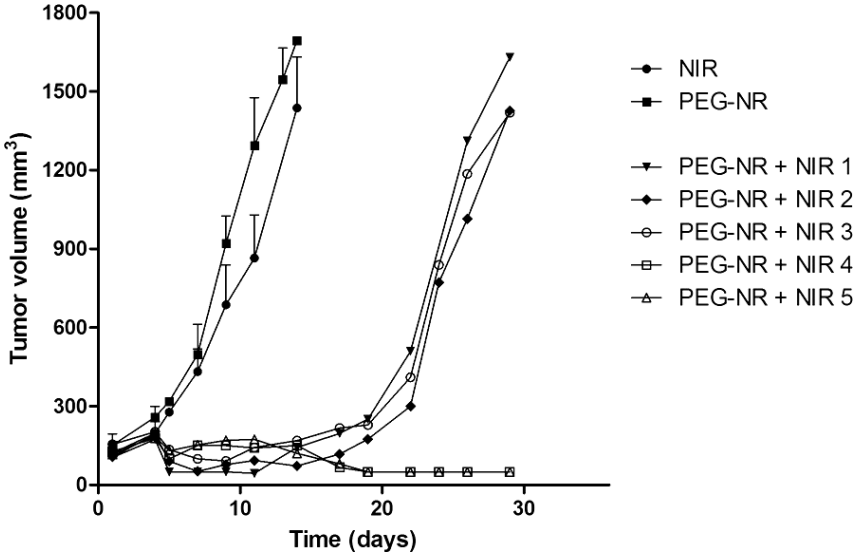

Fig. 5. Photothermal destruction of transgenic sarcoma using PEG-NRs. Volumetric changes in tumor volume are plotted over time ($n = 4$ or 5). Error bars represent standard deviations.